PHYSICAL REVIEW A **89**, 021403(R) (2014)

Control of electronic dynamics visualized by angularly resolved photoelectron spectra: A dynamical simulation with an IR pump and XUV attosecond-pulse-train probe

B. Mignolet,[1] R. D. Levine,[2] and F. Remacle[1,2,*]

[1]*Department of Chemistry, University of Liege, B4000 Liege, Belgium*

[2]*The Fritz Haber Center for Molecular Dynamics, The Hebrew University of Jerusalem, Jerusalem 91904, Israel*

(Received 9 October 2013; published 13 February 2014)

A dynamical simulation via a coupled-equation scheme that includes the ionization continua and field-induced effects describes a pump-probe experiment that monitors ultrafast electronic dynamics in LiH. The ionizing XUV attosecond pulse train that is included in the simulation is used as a frequency filter. By tuning the time interval between the attosecond pulses of the train to a beating frequency of the wave packet induced by the IR pump pulse we characterize the changing spatial localization from one end of the molecule to the other, reflecting the interferences of the nonstationary electronic density.

DOI: 10.1103/PhysRevA.89.021403 PACS number(s): 33.20.Xx, 33.60.+q, 33.80.−b

The development of ultrashort optical pulses has provided ways of probing the electronic dynamics in atoms and molecules [1–5]. Electronic dynamics has been characterized experimentally by high-order-harmonic generation [6–8], attosecond clock measurements [9,10], transient absorption spectroscopy [11,12] and time-resolved molecular-frame photoelectron angular distributions [13]. Until now, however, the electronic dynamics in molecules has been probed indirectly by monitoring the fragments resulting from vibronic couplings to dissociative electronic states [8,14–17] or by measuring the parent ion yield [18].

Pump-probe experiments using a combination of an IR pump pulse with an attosecond-pulse-train (APT) probe have been carried out on atoms [19] and diatomic molecules [15,18]. We show here by dynamical simulation of an IR pump–XUV APT probe experiment with realistic parameters that the spatial localization of the nonstationary electronic wave packet induced by the pump pulse can be probed by time-dependent angularly resolved photoelectron spectra [20]. The APT acts as a frequency filter that only probes the superposition of states with a beating frequency matching the time interval between two XUV attosecond pulses of the train. The time delay between XUV pulses $T/2$, where T is the period of the IR field that generated the APT [21], is ideal to probe electronic states separated by a few eV, which is typically the case for excited states of molecules. So by tuning the frequency of the IR laser, it is possible to selectively probe a given component of the electronic wave packet.

Our dynamical simulation is based on the partitioning technique as applied to the coupled equation scheme [22–29] (see Supplemental Material [30] for details). The projector on the bound subspace consists of the time-independent field-free stationary electronic states $|\Psi_I\rangle$ of the neutral molecule $\mathbf{Q} = \sum_I |\Psi_I\rangle\langle\Psi_I|$. The continuum subspace $\mathbf{P}$, where $\mathbf{P} = \mathbf{1} - \mathbf{Q}$, is composed of antisymmetrized products $|\Psi_K^{\rm cat}, \varepsilon_{\mathbf{k}}^{\perp}\rangle$ of the $n-1$ electron field-free state of the cation $|\Psi_K^{\rm cat}\rangle$ and of the wave function of the electron in channel K, $|\varepsilon_{\mathbf{k}}^{\perp}\rangle$, that is a plane wave orthogonalized to the bound states [31–33]. The imposed orthogonalization ensures that $\mathbf{PQ} = \mathbf{0}$.

The electronic Hamiltonian is expressed at a fixed geometry of the nuclei and also includes the pump and probe pulses [Eq. (1)]. The coupling with the electric field $\mathbf{E}(t)$ is described in the dipole approximation. Atomic units are used throughout the paper, N is the number of nuclei, n is the number of electrons, $\boldsymbol{R}$ denotes the fixed nuclear coordinates, and $\mathbf{r}$ denotes the electronic ones:

$$H(t) = -\sum_{i=1}^{n}\frac{1}{2}\nabla_i^2 - \sum_{\alpha=1}^{N}\sum_{i=1}^{n}\frac{Z_\alpha}{R_{i\alpha}} + \sum_{i}^{n}\sum_{i>j}^{n}\frac{1}{r_{ij}} - \mathbf{E}(t)\sum_{i}^{n}\mathbf{r}_i. \quad (1)$$

Here $\mathbf{E}(t) = -d\mathbf{A}(t)/dt$, where $\mathbf{A}(\mathbf{t})$ has a Gaussian envelope $\mathbf{A}(t) = (f_0/\omega)\exp[-(t-t_0)^2/\sigma^2]\sin(\omega t)$. The partitioned time-dependent Schrödinger equation has the form

$$i\begin{pmatrix} d\mathbf{Q}\Psi(t)/dt \\ d\mathbf{P}\Psi(t)/dt \end{pmatrix} = \begin{pmatrix} \mathbf{Q}H(t)\mathbf{Q} & \mathbf{Q}H(t)\mathbf{P} \\ \mathbf{P}H(t)\mathbf{Q} & \mathbf{P}H(t)\mathbf{P} \end{pmatrix}\begin{pmatrix} \mathbf{Q}\Psi(t) \\ \mathbf{P}\Psi(t) \end{pmatrix}. \quad (2)$$

The bound-state Hamiltonian is the sum of the field-free Hamiltonian $\hat{H}^0_{\rm neut}$ and the time-dependent dipolar coupling, which means that $\mathbf{Q}H(t)\mathbf{Q}$ is nondiagonal:

$$\mathbf{Q}\left(H^0_{\rm neut} - \mathbf{E}(t)\sum_{i=1}^{n}\mathbf{r}_i\right)\mathbf{Q} = \sum_I\sum_J |\Psi_I\rangle\left[E_I^{\rm neut}\delta_{I,J} - \mathbf{E}(t)\mu_{I-J}\right]\langle\Psi_J|. \quad (3)$$

Here μ_{I-J} is the transition dipole matrix element between the field-free n electron states $|\Psi_I\rangle$ and $|\Psi_J\rangle$. The n electron Hamiltonian of the ionized states is approximately written as $H(t) \approx H^{\rm cat}(t) + H^{\rm el}(t)$, where $H^{\rm cat}(t)$ is the $n-1$ electron Hamiltonian of the cation including the $n-1$ dipole interaction $\hat{H}_0^{\rm cat} - \sum_{i=1}^{n-1}\mathbf{E}(t)\mathbf{r}_i$ and $H^{\rm el}(t) = -\frac{1}{2}\nabla^2 - \mathbf{E}(t)\mathbf{r}$. The coupling between the ionized electron and the cation is neglected, as in the strong-field approximation [34]. This coupling plays an important role in tunneling and autoionization [35,36] and leads to further mixing between the bound states and the open ionization channels [37]. It can play a role in the ionization induced by the IR pulse and is not expected to be very large for the fast ionization induced by the APT, which

*Corresponding author: fremacle@ulg.ac.be

dominates the photoelectron spectrum (PES) in the examples discussed below. The effect of the dipolar coupling on the cation field-free states is fully taken into account and leads to the dynamical variation of the ionization potential with the electric field. We also take into account the coupling of the ionized electron to the electric field. The matrix $\mathbf{P}H(t)\mathbf{P}$ is therefore nondiagonal. We show in Ref. [30] how to bring the one-electron part to a diagonal form by a time-dependent unitary transformation of the plane waves, which simplifies considerably the time integration scheme.

The coupling matrix elements between the bound and ionized states, $\mathbf{Q}H(t)\mathbf{P}$ in Eq. (2), can be reduced to a one-electron integral [38], $-\mathbf{E}(t)\int dr\,\Phi_{IK}^{\text{Dyson}}\mathbf{r}\varepsilon_{\mathbf{k}}^{\perp}$, where Φ_{IK}^{Dyson} is the Dyson orbital and corresponds to the overlap between the wave function of the Ith state of the neutral and Kth state of the cation [33,39,40]. We solve the partitioned time-dependent Schrödinger equation [Eq. (2)] by numerical integration to obtain the amplitudes of the wave function $\Psi(t)$ on the bound states $c_I(t)$ and on the states of the $\mathbf{P}$ subspace $c_{K,\mathbf{k}}(t)$. The numerical integration scheme allows using a fine grid for the discretization of the continuum (see [30] for details). In our implementation, the field-free bound electronic states of the neutral and the cation can be computed independently of the time propagation and the level of accuracy of their description can be adapted to the size of the system. For LiH, we use multireference electronic states of Ref. [41]. For larger systems [40,42], methods such as time-dependent density-functional theory (DFT) can be used, which allows us to treat a large band of excited states.

Other theoretical approaches such as grid methods [43–45], many-body S-matrix theory [46], the multiconfiguration time-dependent Hartree-Fock method [47–49], and time-dependent multiconfiguration self-consistent field theory [50,51] have been used to describe the electron dynamics in strong fields. These methods are often limited to small systems and/or confined in one dimension, but they allow us to include the nuclear motion for simple diatomic or triatomic molecules [43,49,52–54]. The ultrafast electron-nuclear dynamics can also be computed at the mean-field level using time-dependent DFT [55].

To demonstrate the efficiency of the probing setup that we propose, we simulate a pump-probe experiment on the LiH molecule [20,41,56–58] as closely as possible to what can be currently achieved experimentally using short and ultrashort pulses. LiH can be oriented due to the large permanent dipole moment (2.1 D) of its ground state (GS) [59,60] and the nuclear dynamics is not expected to be important in the first dozen femtoseconds [49] following the excitation. We first report on the electronic dynamics induced by a 5-fs IR pulse and probed by an XUV APT. We then investigate the dynamics induced by a longer IR pulse (20 fs) and probed by an APT at short times, before the nuclear motion starts to interfere with the electronic dynamics.

In the first example, a 5-fs 800-nm IR pulse polarized in the (x,z) plane of the molecular frame, where z is the molecular axis [see Fig. 1(b)], is used to create a coherent superposition of the GS (Σ symmetry) and the lowest Σ and Π (1Σ and 1Π) excited states. These states are respectively 3.11 and 3.87 eV above the GS and can be reached by two IR photons [Fig. 1(a)]. The pulse strength corresponds to a Keldysh parameter [61]

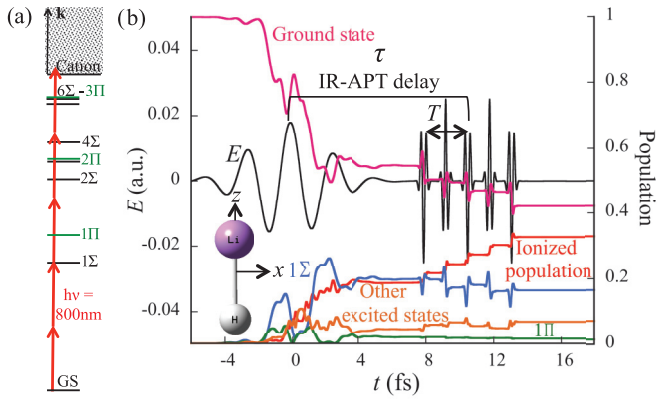

FIG. 1. (Color online) (a) The IR excitation scheme of the ten lowest electronic Σ (black) and Π (green) states of LiH that are below the IP. (b) Electronic dynamics induced by an IR pulse ($\omega = 0.057$ a.u., $f_0 = 0.018$ a.u., and $\sigma = 125$ a.u.) polarized in the (x,z) plane (the orientation of LiH in the Cartesian axis of the molecular frame is shown in the inset) and by an APT ($f_0 = 0.025$ a.u., $\sigma = 8$ a.u., and $\omega = 0.4$ a.u.) generated from a 800-nm laser and polarized along z. The pump probe delay τ is defined as the time delay between the IR pump field and the middle of the pulse train. Two XUV pulses with the same phase are separated by the period T of the IR field.

of 2.4, which indicates that photoionization is the dominant process. Higher excited states are also significantly populated during the IR pulse [Fig. 1(b)] because they have strong dipolar coupling with the excited 1Σ and 1Π states. These states have large photoionization widths [55] and act as doorway states for the ionization by the IR pump pulse.

The complex dynamics induced by the IR pulse is probed by an APT generated by 800-nm radiation, composed of five XUV pulses of 0.3 fs separated by 1.32 fs, which corresponds to half the period of the IR field [21] and also to the beating period between the GS and the 1Σ states. Because of the period matching between $T/2$ and $h/\Delta E_{\text{GS}-1\Sigma}$, the APT acts as a filter and each of the five pulses probes the same phase relations between the states of the electronic wave packet, which gives a clear picture of the electronic dynamics. At each pump-probe delay τ, the electrons will be preferentially emitted toward the top (Li atom) or the bottom (H atom) along the z axis, depending on the phase of the superposition of states. This will be reflected in the anisotropy parameter

$$Y^{-z,+z}(\varepsilon,\tau) = [P_{\text{down}}(\varepsilon,\tau) - P_{\text{up}}(\varepsilon,\tau)]/[P_{\text{up}}(\varepsilon,\tau) + P_{\text{down}}(\varepsilon,\tau)],$$

where $P_{\text{up}}(\varepsilon,\tau)$ and $P_{\text{down}}(\varepsilon,\tau)$ are the fraction of electrons collected at the top and bottom detectors, respectively, for a given kinetic energy ε and a given delay time τ. These fractions are computed by integration of the population $|c_{K,\mathbf{k}}(t)|^2$ at a kinetic energy $\varepsilon = \mathbf{k}^2/2$ for positive P_{up} and negative P_{down} values of the z component of the momentum vector k_z, respectively. The PES shown in Fig. 2(a) is obtained by integrating the population of the ionized states at the end of the pulse over all the orientations for each kinetic energy. The photoelectron ionized during the pump pulse and the ones resulting from the ionization by the train of XUV both contribute to the PES. The electrons photoionized by the train

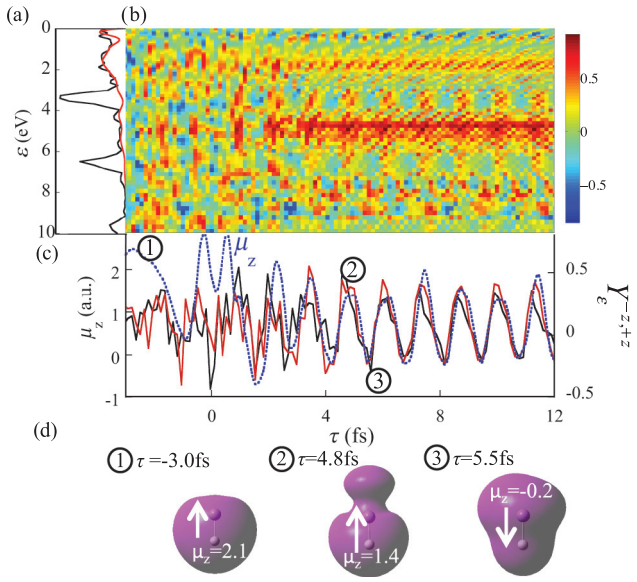

FIG. 2. (Color online) (a) Photoelectron spectrum computed for the ionization induced by the IR pump pulse only (red) and by both the IR pulse and the APT (black). (b) Heat map $Y^{-z,+z}(\varepsilon,\tau)$ computed as a function of τ and ε, with the pulse parameters used in Fig. 1 and an APT generated by a 800-nm IR laser resonant with the GS-1Σ period. (c) Time-dependent response of $\mu_z(\tau)$, the z component of the dipole moment (blue dotted lines), and $Y_\varepsilon^{-z,+z}(\tau)$ for ε in the ranges 3.0–3.8 eV (black) and 6.1–6.8 eV (red), which correspond to the two mains peaks of the PES in (a). (d) The electron densities computed at different delay times as indicated show different localizations, in agreement with the beating of $Y_\varepsilon^{-z,+z}(\tau)$ and $\mu_z(\tau)$.

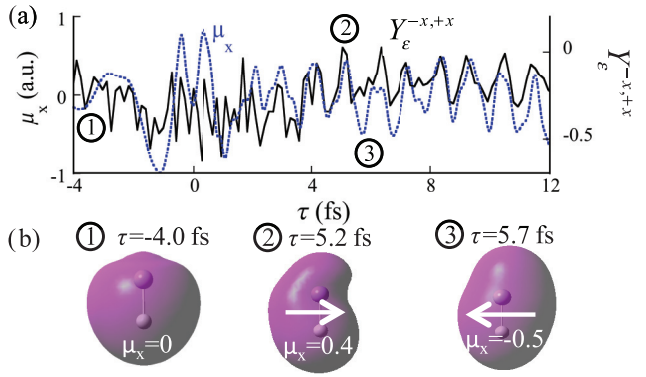

FIG. 3. (Color online) (a) Time-dependent response of $\mu_x(\tau)$ and $Y_\varepsilon^{-x,+x}(\tau)$ corresponding to the main peak of the PES (see Fig. S1 in [30]) computed for an APT generated by a 638-nm laser, resonant with the GS-1Π period of 1.06 fs. (b) Electron densities computed at delay times as indicated show different localizations, in agreement with the beating of $Y_\varepsilon^{-x,+x}(\tau)$ and $\mu_x(\tau)$.

of XUV pulses have a specific kinetic energy that corresponds to the ionization by the harmonics of the APT, which are separated by 3.1 eV and extend up to 30 eV. This leads to the narrow peaks in the PES, which are superimposed on the broad peak due to the IR pulse [Fig. 2(a)]. A heat map of the anisotropy parameter $Y^{-z,+z}(\varepsilon,\tau)$ computed as a function of ε and τ is shown in Fig. 2(b) for pump-probe delays ranging from -3 to 12 fs. For kinetic energies that correspond to peaks in the PES, $Y^{-z,+z}(\varepsilon,\tau)$ clearly beats with the same frequency as the dipole moment [see Fig. 2(c)], while for the other kinetic energies, there is no clear beating frequency. This is better seen in Fig. 2(c), where we show $Y_\varepsilon^{-z,+z}(\tau)$, the value of $Y^{-z,+z}(\varepsilon,\tau)$ integrated over the range of kinetic energies of PES peaks as well as the time-dependent response of the z component of the dipole moment $\mu_z(t)$. The dipole moment is an observable over the time-dependent electronic density and reflects its localization at the time of probing by the APT. The beating periods in $\mu_z(t)$ correspond to the transition frequencies of the nonstationary electronic wave packet [41,56,57]. There is no significant beating of $Y_\varepsilon^{-z,+z}(\tau)$ and $\mu_z(t)$ when the probing train of XUV pulses precedes the IR pulse. The beatings start for $\tau > 2$ fs when the IR pulse is strong enough to form a coherent superposition of excited states of the neutral. During the pulse, the transient dynamics is complex, which is reflected by several beating frequencies in $\mu_z(t)$ and $Y_\varepsilon^{-z,+z}(\tau)$. When the IR pump pulse is over, for $\tau > 4$ fs, the dynamics is field free. Then, as can be seen from time-dependent densities of Fig. 2(c), an accumulation of electronic density close to the Li corresponds to a negative value of the dipole moment and a negative value of the anisotropy parameter such that the ionization occurs preferentially from the Li when the density is localized on it.

For probing other components of the wave packet, the $T/2$ period of the APT can be adjusted by tuning the frequency of the IR laser [62–64]. For example, the beating between the GS and 1Π states induced by excitation using the same IR pump pulse can be probed by an APT generated from a 638-nm laser. Because the 1Π state has a higher excitation energy than the 1Σ state, the beating will be faster with a period of 1.06 fs. The beating between the GS and the 1Π states occurs perpendicularly to the molecular axis, so we computed $Y_\varepsilon^{-x,+x}(\tau)$ along x [Fig. 3(a)] for the main peak of the PES. Even for the 3% of the system in the 1Π state, we still observe a clear beating of the anisotropy parameter, which correlates with the beating of $\mu_x(t)$ and with the motion of the electron density [Fig. 3(b)]. When the system is probed by an APT with a $T/2$ that does not correspond to a specific beating period between two states, we do not observe beatings of the anisotropy parameter (see Fig. S2 in [30]).

By varying systematically the delay time between two pulses of an APT, one can therefore characterize the field-free excited states that take part in the time-evolving electronic wave packet induced by a short IR pulse and probe the localization of the electron density. This superposition can be tuned using the parameters of the IR pulse [41,57]. The strength (2×10^{13} W/cm^2) of the XUV APT used to compute Figs. 2 and 3 is chosen to have a clear XUV ionization signal compared to the ionization induced by the IR pulse [Fig. 2(a)]. In the simpler case of a weaker XUV APT that does not induce bound-state dynamics, one can subtract the IR background to analyze the anisotropy parameter.

A recent pump-probe experiment using a long IR pulse with an overlapping APT to probe small polyatomic molecules showed that the parent ion yield varies with the time delay between the pump and probe pulse [18]. Such a long pulse is expected to launch complex electronic dynamics in the bound

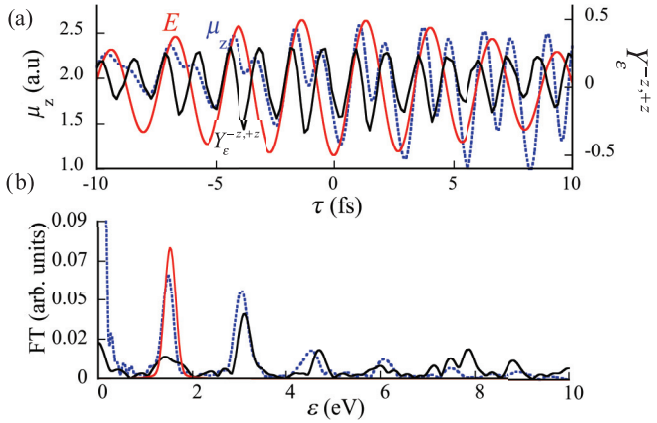

FIG. 4. (Color online) (a) Time-dependent response of $\mu_z(\tau)$ (dotted blue lines), $Y_\varepsilon^{-z,+z}(\tau)$ (black solid lines), and the electrical field E (red solid lines) computed for a 20-fs IR pulse ($\omega = 0.057$, $f_0 = 0.005$ a.u., and $\sigma = 500$ a.u.) and the probing APT of Fig. 1(b). (b) Fourier transform of the pulse (single red peak at 1.55 eV) of $\mu_z(\tau)$ (dotted blue line) and of $Y_\varepsilon^{-z,+z}(\tau)$ (black solid line).

states, with coupling to the nuclei dynamics after a dozen fs. We show in Fig. 4 that one can use the anisotropy parameter $Y_\varepsilon^{-z,+z}(\tau)$ resulting from the probing by an APT at short delay times to analyze the electron dynamics. In Fig. 4, $Y_\varepsilon^{-z,+z}(\tau)$ is computed for a long 20-fs IR pump pulse. At the beginning of the pulse, when the IR field is weak, the electrons adapt adiabatically to the field and the dipole moment $\mu_z(\tau)$ follows the oscillations of the field [Fig. 4(a)]. The APT at 800 nm mainly probes the dynamics between the GS and the 1Σ state, but also between the GS and the 4Σ state that is slightly populated. At longer times, the field is strong enough to induce complex dynamics in the bound states and the dipole moment beats with several frequencies that can be characterized by a Fourier transform. We show the Fourier transform of $E(\tau)$, $\mu_z(\tau)$, and $Y_\varepsilon^{-z,+z}(\tau)$ in Fig. 4(b). As expected, we get a single peak at 1.55 eV for $E(\tau)$. Both $\mu_z(\tau)$ and $Y_\varepsilon^{-z,+z}(\tau)$ also show a peak at the one-photon energy, which reflects that the electron density of the GS adiabatically follows the oscillations of the electric field. However, for $\mu_z(\tau)$ and $Y_\varepsilon(\tau)$, a strong peak is observed at the two-photon energy (3.1 eV), which reflects the GS-1Σ period. The weaker peak at the four-photon energy (6.20 eV) is resonant with the GS-4Σ transition frequency. The APT at 800 nm therefore identifies the 1Σ and 4Σ states in the electronic wave packet. By tuning the period $T/2$ between the pulses of the train using different IR frequencies, one could systematically characterize the superposition of states created by the IR pulse.

In conclusion, the nonstationary electron dynamics that can be set in motion by an ultrashort IR pulse can be probed by angularly resolved ultrafast ionization induced by a train of attosecond pulses that is used as a frequency filter.

F.R. and B.M. gratefully acknowledge support from the Fonds de la Recherche Fondamentale Collective, Grant No. 2.4545.12, and from the Fonds National de la Recherche Scientifique (Belgium). F.R. and R.D.L. thank the Einstein Foundation of Berlin.

[1] M. F. Kling and M. J. J. Vrakking, Annu. Rev. Phys. Chem. **59**, 463 (2008).
[2] P. B. Corkum and F. Krausz, Nat. Phys. **3**, 381 (2007).
[3] F. Krausz and M. Ivanov, Rev. Mod. Phys. **81**, 163 (2009).
[4] F. Lépine, G. Sansone, and M. J. J. Vrakking, Chem. Phys. Lett. **578**, 1 (2013).
[5] P. Wernet, Phys. Chem. Chem. Phys. **13**, 16941 (2011).
[6] Y. Mairesse *et al.*, Phys. Rev. Lett. **104**, 213601 (2010).
[7] O. Smirnova, Y. Mairesse, S. Patchkovskii, N. Dudovich, D. Villeneuve, P. Corkum, and M. Y. Ivanov, Nature (London) **460**, 972 (2009).
[8] X. Zhou, P. Ranitovic, C. W. Hogle, J. H. D. Eland, H. C. Kapteyn, and M. M. Murnane, Nat. Phys. **8**, 232 (2012).
[9] A. N. Pfeiffer, C. Cirelli, M. Smolarski, and U. Keller, Chem. Phys. **414**, 84 (2013).
[10] P. Eckle, A. N. Pfeiffer, C. Cirelli, A. Staudte, R. Dörner, H. G. Muller, M. Büttiker, and U. Keller, Science **322**, 1525 (2008).
[11] E. Goulielmakis *et al.*, Nature (London) **466**, 739 (2010).
[12] M. Holler, F. Schapper, L. Gallmann, and U. Keller, Phys. Rev. Lett. **106**, 123601 (2011).
[13] P. Hockett, C. Z. Bisgaard, O. J. Clarkin, and A. Stolow, Nat. Phys. **7**, 612 (2011).
[14] M. F. Kling *et al.*, Science **312**, 246 (2006).
[15] G. Sansone *et al.*, Nature (London) **465**, 763 (2010).
[16] W. Li, A. A. Jaron-Becker, C. W. Hogle, V. Sharma, X. Zhou, A. Becker, H. C. Kapteyn, and M. M. Murnane, Proc. Natl. Acad. Sci. U.S.A. **107**, 20219 (2010).
[17] S. Haessler *et al.*, Nat. Phys. **6**, 200 (2010).
[18] C. Neidel *et al.*, Phys. Rev. Lett. **111**, 033001 (2013).
[19] J. Mauritsson *et al.*, Phys. Rev. Lett. **105**, 053001 (2010).
[20] B. Mignolet, R. D. Levine, and F. Remacle, Phys. Rev. A **86**, 053429 (2012).
[21] J. Mauritsson, P. Johnsson, E. Gustafsson, A. L'Huillier, K. J. Schafer, and M. B. Gaarde, Phys. Rev. Lett. **97**, 013001 (2006).
[22] R. D. Levine, *Quantum Mechanics of Molecular Rate Processes* (Clarendon, Oxford, 1969).
[23] P. Rivière, A. Palacios, J. Pérez-Torres, and F. Martín, in *Progress in Ultrafast Intense Laser Science VIII*, edited by K. Yamanouchi, M. Nisoli, and W. T. Hill III (Springer, Berlin, 2012), Vol. 103, p. 1.
[24] J. L. Sanz-Vicario, J. F. Pérez-Torres, F. Morales, E. Plésiat, and F. Martín, Int. J. Quantum Chem. **110**, 2462 (2010).
[25] R. E. F. Silva, P. Rivière, and F. Martín, Phys. Rev. A **85**, 063414 (2012).
[26] S. Selstø, A. Palacios, J. Fernández, and F. Martín, Phys. Rev. A **75**, 033419 (2007).
[27] Y. Arasaki and K. Takatsuka, ChemPhysChem **14**, 1387 (2013).
[28] F. H. M. Faisal, *Theory of Multiphoton Processes* (Plenum, New York, 1987).
[29] C. Cohen-Tannoudji, J. Dupont-Roc, and G. Grynberg, *Atom-Photon Interactions* (Wiley-VCH, Weinheim, 2008).

[30] See Supplemental Material at http://link.aps.org/supplemental/10.1103/PhysRevA.89.021403 for details of the partitioning technique as applied to the couple-equation scheme and for the supplemental figures S1 and S2.
[31] M. Deleuze, B. T. Pickup, and J. Delhalle, Mol. Phys. **83**, 655 (1994).
[32] F. O. Ellison, J. Chem. Phys. **61**, 507 (1974).
[33] G. M. Seabra, I. G. Kaplan, V. G. Zakrzewski, and J. V. Ortiz, J. Chem. Phys. **121**, 4143 (2004).
[34] H. R. Reiss, Phys. Rev. A **22**, 1786 (1980).
[35] O. Smirnova, M. Spanner, and M. Ivanov, Phys. Rev. A **77**, 033407 (2008).
[36] A. Staudte *et al*., Phys. Rev. Lett. **102**, 033004 (2009).
[37] L. Torlina, M. Ivanov, Z. B. Walters, and O. Smirnova, Phys. Rev. A **86**, 043409 (2012).
[38] S. Patchkovskii, Z. Zhao, T. Brabec, and D. M. Villeneuve, J. Chem. Phys. **126**, 114306 (2007).
[39] H. Reisler and A. I. Krylov, Int. Rev. Phys. Chem. **28**, 267 (2009).
[40] B. Mignolet, T. Kùs, and F. Remacle, in *Imaging and Manipulating Molecular Orbitals*, edited by L. Grill and C. Joachim (Springer, Berlin, 2013), p. 41.
[41] F. Remacle and R. D. Levine, Phys. Rev. A **83**, 013411 (2011).
[42] B. Mignolet, J. O. Johansson, E. E. B. Campbell, and F. Remacle, ChemPhysChem **14**, 3332 (2013).
[43] A. D. Bandrauk, S. Chelkowski, S. Kawai, and H. Z. Lu, Phys. Rev. Lett. **101**, 153901 (2008).
[44] A. D. Bandrauk, S. Chelkowski, and H. S. Nguyen, Int. J. Quantum Chem. **100**, 834 (2004).
[45] F. L. Yip, A. Palacios, T. N. Rescigno, C. W. McCurdy, and F. Martín, Chem. Phys. **414**, 112 (2013).
[46] A. Becker and F. H. M. Faisal, Phys. Rev. Lett. **84**, 3546 (2000).
[47] J. Caillat, J. Zanghellini, M. Kitzler, O. Koch, W. Kreuzer, and A. Scrinzi, Phys. Rev. A **71**, 012712 (2005).
[48] T. Kato and H. Kono, Chem. Phys. **366**, 46 (2009).
[49] I. S. Ulusoy and M. Nest, J. Chem. Phys. **136**, 054112 (2012).
[50] T. T. Nguyen-Dang, M. Peters, S.-M. Wang, E. Sinelnikov, and F. Dion, J. Chem. Phys. **127**, 174107 (2007).
[51] T. T. Nguyen-Dang, M. Peters, S. M. Wang, and F. Dion, Laser Phys. **19**, 1521 (2009).
[52] B. H. Muskatel, F. Remacle, and R. D. Levine, J. Phys. Chem. A **116**, 11311 (2012).
[53] M. Spanner *et al*., J. Phys. B **45**, 194011 (2012).
[54] H. Kono, Y. Sato, N. Tanak, T. Kato, K. Nakai, S. Koseki, and Y. Fujimura, Chem. Phys. **304**, 203 (2004).
[55] U. De Giovannini, G. Brunetto, A. Castro, J. Walkenhorst, and A. Rubio, ChemPhysChem **14**, 1363 (2013).
[56] B. Mignolet, A. Gijsbertsen, M. J. J. Vrakking, R. D. Levine, and F. Remacle, Phys. Chem. Chem. Phys. **13**, 8331 (2011).
[57] F. Remacle, M. Nest, and R. D. Levine, Phys. Rev. Lett. **99**, 183902 (2007).
[58] M. Nest, F. Remacle, and R. D. Levine, New J. Phys. **10**, 025019 (2008).
[59] O. Ghafur, A. Rouzee, A. Gijsbertsen, W. K. Siu, S. Stolte, and M. J. J. Vrakking, Nat. Phys. **5**, 289 (2009).
[60] P. M. Kraus, A. Rupenyan, and H. J. Wörner, Phys. Rev. Lett. **109**, 233903 (2012).
[61] L. V. Keldysh, Zh. Eksp. Teor. Fiz. **47**, 1945 (1964) [Sov. Phys. JETP **20**, 1307 (1965)].
[62] F. Frassetto, C. Cacho, C. A. Froud, I. C. E. Turcu, P. Villoresi, W. A. Bryan, E. Springate, and L. Poletto, Opt. Express **19**, 19169 (2011).
[63] F. Frassetto, P. Villoresi, and L. Poletto, J. Opt. Soc. Am. A **25**, 1104 (2008).
[64] L. Poletto, P. Villoresi, E. Benedetti, F. Ferrari, S. Stagira, G. Sansone, and M. Nisoli, Opt. Lett. **32**, 2897 (2007).